Water Research 283 (2025) 123852

Contents lists available at ScienceDirect

Water Research

journal homepage: www.elsevier.com/locate/watres

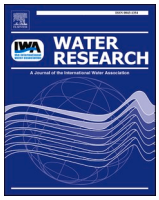

Enhanced removal of organic micropollutants using 2D metal-organic framework interlayered nanofiltration membrane

Ruiying Li, Lingyue Zhang *, Shuang Zheng, Wenyu Liu, Li Long, Chuyang Tang *

Department of Civil Engineering, The University of Hong Kong, Pokfulam, Hong Kong Special Administrative Region of China

ARTICLE INFO

Keywords:
Interlayers
Metal-organic frameworks (MOFs)
Nanofiltration membranes
Organic micropollutants
Polyamide

ABSTRACT

Organic micropollutants (OMPs) present considerable threats to both human health and the environment. Traditional thin film composite (TFC) nanofiltration (NF) polyamide membranes, despite their high water permeance and salt rejection capabilities, often fail to effectively remove OMPs. This study addresses this limitation by incorporating two-dimensional (2D) zinc(II) tetrakis(4-carboxy-phenyl)porphyrin (Zn-TCPP) metal-organic framework (MOF) nanosheets as interlayers in TFC membranes (TFNi), using a polyethylene glycol (PEG) assisted exfoliation technique to mitigate issues of nanosheet restacking and aggregation. The uniformly distributed MOF interlayers significantly improved pure water permeance from 10.6 to 32.1 L m^{-2} h^{-1} bar^{-1} while maintaining a high rejection of 97.0% towards Na_2SO_4. Moreover, the optimized membrane showed significant improvements in OMP removal, attributed to the increased negative charge and greater hydrophilicity of the polyamide rejection layer. These findings highlight the potential of 2D MOF nanosheets as interlayers in developing high-performance membranes for effective OMP removal and water reuse.

1. Introduction

The presence of organic micropollutants (OMPs) such as pharmaceutically active compounds (PhACs), endocrine-disrupting chemicals (EDCs), and poly- and perfluoroalkyl substances (PFASs) has raised significant global concerns regarding aquatic safety (Bhatt et al., 2022; Tran et al., 2018; Zhao et al., 2023). These persistent contaminants enter water bodies through various pathways, including domestic wastewater and industrial effluents (Eggen et al., 2014; Luo et al., 2014). Despite trace levels of OMPs found in water ranging from ng/L to μg/L, the increasing quantities of these pollutants have heightened concerns due to their toxicological impacts on both aquatic ecosystems and human health (Barbosa et al., 2016; Garg et al., 2020; Lapworth et al., 2012; Price et al., 2010). Compounding these challenges, many OMPs exhibit molecular weights of <500 Da and diverse physicochemical properties (e.g., charge and hydrophobicity), rendering them poorly removed by the traditional water treatment methods (Guo et al., 2022; Khanzada et al., 2020; Luo et al., 2014). Consequently, it is imperative to implement effective remediation strategies to effectively remove OMPs.

Thin film composite (TFC) polyamide (PA) nanofiltration (NF) membranes are widely utilized in contemporary water treatment processes for water reuse and purification (Ahmad et al., 2022; Lau et al., 2015; Tang et al., 2018; Zhou et al., 2023). Although these NF membranes show high rejection for divalent salts, they are less effective at removing OMPs, particularly those neutral low-molecular weight compounds (Guo et al., 2022; Liu et al., 2022). This reduced efficiency is often attributed to unfavorable interactions such as hydrophobic interaction between the membrane and the solutes (Braeken et al., 2005; Guo et al., 2016; Kimura et al., 2003; Schafer et al., 2011).

To improve OMP rejection by TFC membranes, it is crucial to improve membrane selectivity (Guo et al., 2022; Liu et al., 2023). Recent studies have shown that incorporating interlayers within TFC membranes can significantly accelerate water transport (thereby increasing water permeance) and simultaneously enhance salt retention (resulting in decreased solute permeance) (Dai et al., 2020; Wang et al., 2023; Zhao et al., 2021). These insightful findings prompt us to investigate whether water/OMP selectivity could be enhanced in TFC membranes with interlayered structures (TFNi).

Various nanomaterials have been investigated as interlayers including graphene oxide, MXene, and carbon nanotubes (Ji et al., 2021; Long et al., 2022; Wang et al., 2021; Xu et al., 2020). Compared to these nanomaterials, two-dimensional (2D) metal-organic framework (MOF) nanosheets present distinct advantages as interlayers. They provide a hydrophilic surface conducive to forming a thin polyamide rejection

* Corresponding authors.
E-mail addresses: zly17@hku.hk (L. Zhang), tangc@hku.hk (C. Tang).

https://doi.org/10.1016/j.watres.2025.123852
Received 8 March 2025; Received in revised form 3 May 2025; Accepted 16 May 2025
Available online 18 May 2025

layer (Wen et al., 2020). Besides, their ultrathin thickness and high porosity minimize water transport resistance (Cheng et al., 2024), making them promising interlayers for high-performance TFC membranes (Alemayehu et al., 2022; Li et al., 2017; Wang et al., 2022). Nevertheless, the development of high-performance 2D MOF TFNi membranes encounters several challenges. Conventional ultrasonic-assisted methods yield low quantities of MOF nanosheets (Jin et al., 2023; Li et al., 2011; Rodenas et al., 2015). The restacking and aggregation of these exfoliated nanosheets may also hinder membrane formation and deteriorate performance. Additionally, most studies on MOF TFNi membranes primarily focus on enhancing water permeance and salt rejection (Cheng et al., 2022), with a lack of comprehensive research exploring the potential of 2D MOF nanosheets to elucidate the mechanisms involved in the removal of OMPs.

In this study, we developed a highly selective 2D zinc(II) tetrakis(4-carboxy-phenyl)porphyrin (Zn-TCPP) MOF TFNi membrane. MOF nanosheets were prepared by a novel polyethylene glycol (PEG) assisted exfoliation method to prevent their aggregation. The resulting uniform MOF interlayer was utilized to synthesize the polyamide rejection layer via interfacial polymerization (IP). We systematically investigated the impact of these interlayers on membrane formation and transport characteristics for removing OMPs, specifically targeting PhACs, EDCs, and PFASs. Moreover, the mechanisms underlying the enhanced OMP removal capabilities of the MOF TFNi membrane were elucidated. The role of the interlayer in improving water-OMPs selectivity was thoroughly investigated, framed within the context of the membrane's structure-property-performance relationship. This study provides valuable insights into employing 2D MOF nanosheets in constructing TFNi membranes toward efficient OMP removal.

2. Experimental

2.1. Materials and chemicals

In this study, all the chemicals with analytical grades were used without further purification. Zinc nitrate hexahydrate ($Zn(NO)_3.6H_2O$, 98%), tetrakis(4-carboxyphenyl)porphyrin (TCPP, 97%), pyrazine, polyethylene glycol (PEG, Mn~20,000), dimethylformamide (DMF, 98%) and ethanol (99%) were obtained from Sigma-Aldrich and were used for the synthesis of Zn-TCPP MOF nanosheet. A polyethersulfone (PES) ultrafiltration membrane with a MWCO of 20,000 Da (UP020) was chosen as the substrate to prepare NF membranes. Piperazine (PIP, 99%) and trimesoyl chloride (TMC, 98%) purchased from Sigma-Aldrich were used for the IP reaction to obtain the polyamide rejection layer. Sodium chloride (NaCl, 99%) and sodium sulfate (Na_2SO_4, 99%) used in salt rejection were purchased from Dieckmann. Four PFASs, four EDCs, and three PhACs (Table S1) were investigated in the OMPs removal test. Five neutral molecules (Table S1) were applied to determine the membrane pore size and molecular weight cutoff.

2.2. Preparation of Zn-TCPP MOF nanosheets

Zn-TCPP MOF nanosheets were synthesized using a PEG-assisted approach (Fig. 1A). $Zn(NO)_3.6H_2O$ (13.5 mg), pyrazine (2.4 mg) and PEG (360 mg) were fully dissolved in 36 mL DMF and ethanol mixture (v:v = 3:1). Subsequently, TCPP (12 mg) dissolved in 12 mL mixture of DMF and ethanol (v:v = 3:1) was dropwise added. The mixed solution was kept stirring at 65°C for 1 day, and then the collected nanosheets were thoroughly washed with ethanol and centrifuged at 10,000 rpm for 10 min. This process was repeated at least three times. Additionally, the same amounts of PEGs with different molecular weights (Mn ~ 600, 4000, and 10,000 g/mol) were employed in the MOF exfoliation process to observe differences in morphology.

2.3. Fabrication of NF membranes with MOF interlayer

To prepare the MOF interlayer, the synthesized Zn-TCPP (8 mg) nanosheets were well dispersed in 800 mL ethanol and subjected to sonication to achieve a homogeneous solution before being loaded onto the substrate. Then, different amounts of Zn-TCPP were loaded onto the PES substrate by filtering a certain volume of the aforementioned suspension (0 mL, 12.5 mL, 25 mL, 50 mL, 100 mL). To synthesize the polyamide rejection layer, IP was performed on the modified MOF-PES support (Fig. 1B). The substrate was first soaked in 20 mL 0.2 wt.% PIP/H_2O solution for 1 min, and then the solution was completely vacuum filtered through the substrate. This vacuum-assisted process can

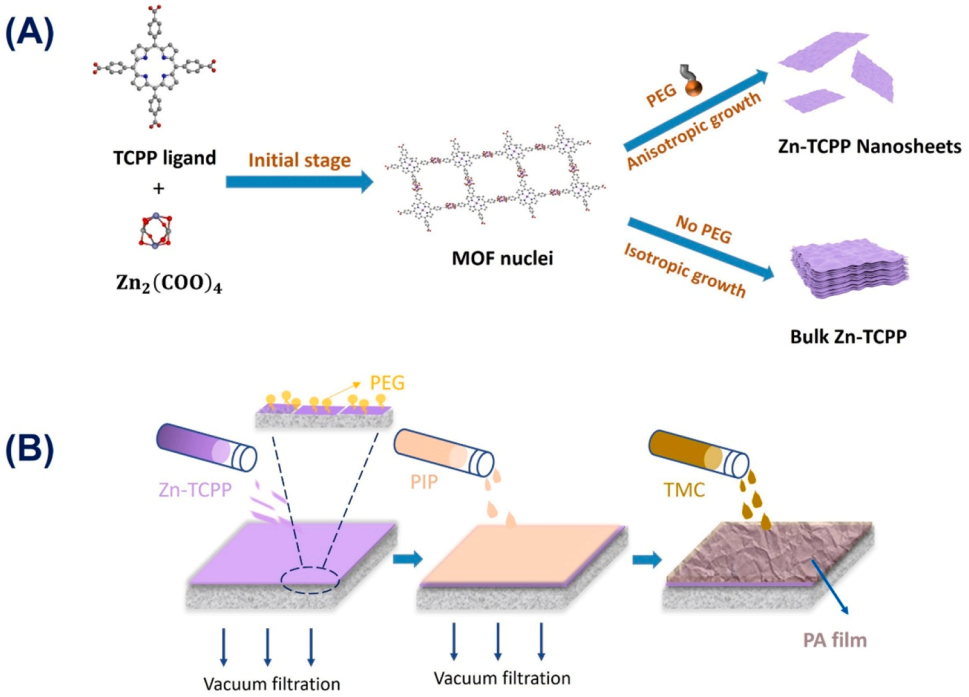

Fig. 1. Schematics of (A) exfoliation of MOF nanosheets and (B) fabrication of NF membranes.

facilitate a more uniform distribution of PIP monomers in the substrate (Fang et al., 2024; Zhu et al., 2020). Next, the PIP-impregnated support was exposed to a 20 mL 0.1 wt.% TMC/hexane solution for 90 s to conduct the IP reaction. The resultant membranes were thoroughly rinsed with pure hexane to remove the residues and dried at room temperature. The fabricated NF membranes were denoted as NF-x membranes, with x presenting the filtration volume of the MOF suspension. To exclude the influence of PEG, an additional TFC membrane without MOF interlayer was fabricated. This membrane, denoted as NF-0-PEG, was produced by incorporating 360 mg PEG into the PIP solution during the IP reaction.

2.4. Characterization

The morphology and lamellar structure of the synthesized MOF nanosheets were observed using transmission electron microscopy (TEM, G2, FEI Tecnai). The crystal structure of the Zn-TCPP was examined by X-ray diffraction (XRD, D8, Bruker), scanning from 5° to 40° (angle 2θ) with a step of 0.02°. The thickness of the Zn-TCPP nanosheet was evaluated by an atomic force microscope (AFM, Dimension Icon, Bruker).

The membrane morphologies were characterized using field emission scanning electron microscopy (FE-SEM, S-4800, Hitachi) and TEM (G2, FEI Tecnai). The functional groups on the membrane surface were determined by an attenuated total reflection Fourier transform infrared spectroscopy (ATR-FTIR, iD5, Thermo Scientific). An X-ray photoelectron spectrometer (XPS, K-Alpha, Thermo Scientific) was used to analyze the elemental compositions of the membrane surface. The AFM (Dimension Icon, Bruker) was applied to evaluate the roughness of the membrane surface. An optical goniometer (Attension Theta, Biolin Scientific) was employed to measure the water contact angle of the membrane surface. A zeta potential analyzer (SurPASS 3, Anton Paar) was used with 1 mM KCl solution as the background electrolyte to determine the membrane surface charge.

2.5. Filtration experiments

The NF membrane filtration experiments were conducted using a homemade crossflow filtration system at 25°C. Before the measurements, the membranes with an effective area of 2 cm^2 were pre-compacted under 5 bar with a crossflow rate of 16.7 cm/s for 2 h to reach a stable flux. All the filtration experiments were performed at least three times.

Salt rejection of the membrane was performed using 1000 ppm Na_2SO_4 or NaCl as the feed solution (pH 6.7±0.2). The concentrations of the salt in the collected permeate were determined by a conductivity meter (Ultrameter II, Myron L). The membrane rejection of neutral probes, such as dextran, raffinose, sucrose, glucose, and glycerol (Table S1), was tested using a feed concentration of 200 ppm. Their permeate concentrations were measured using a total organic carbon analyzer (TOC-L CPH, Shimadzu).

The rejection of OMPs including PFASs, EDCs, and PhACs (Table S1) was tested using a cocktail of all OMPs with a feed concentration of 200 ppb. A concentration of 600 ppm of NaCl was included in the feed solution to mimic the typical ionic strength levels relevant to water reuse scenarios (Liu et al., 2023). The permeate samples were collected after 6 h of filtration to reach stable rejections of OMPs. We performed additional tests over 48 h, and stable rejections of OMPs were obtained (Fig. S1). This suggests that 6 h of filtration is sufficient for the determination of steady-state rejections. The OMP concentrations were measured by liquid chromatography with tandem mass spectrometry (LC-MS/MS, 1290 Infinity, Agilent; 3200 QTRAP, AB SCIEX). The analysis method and the detailed settings of LC-MS/MS can be found in our previous work (Guo et al., 2017).

The water flux J_w (L m^{-2} h^{-1}), the water permeance of the membrane A (L m^{-2} h^{-1} bar^{-1}), membrane rejection R (%), and solute permeance B (L m^{-2} h^{-1}) are determined by Eqs. (1), (2), (3), and (4) respectively:

$$J_w = \frac{\Delta V}{S \times \Delta t} \tag{1}$$

$$A = \frac{J_w}{(\Delta P - \Delta \pi)} \tag{2}$$

$$R = 1 - \frac{C_p}{C_f} \tag{3}$$

$$B = J_w \times \left(\frac{1}{R} - 1\right) \tag{4}$$

where ΔV (L) is the volume of the collected water permeate during a certain time Δt (h), S (m^2) is the effective membrane filtration area, ΔP (bar) is the applied pressure, $\Delta \pi$ (bar) is the osmotic pressure difference across the membrane, C_f and C_p are the concentrations of the solutes in the feed and permeate respectively.

3. Results and discussion

3.1. Exfoliation of Zn-TCPP MOF nanosheets

The Zn-TCPP MOF was exfoliated using the PEG-assisted approach (Fig. 1A). The tetragonal structure of the exfoliated Zn-TCPP MOF nanosheets was confirmed by the XRD results (Fig. 2A), which revealed four distinct peaks corresponding to its (100), (110), (002), and (004) crystallographic planes. Compared to the XRD spectra of bulk Zn-TCPP (Fig. S2), the tetragonal crystalline structure of the Zn-TCPP nanosheets remained intact after exfoliation.

The structural compositions of the Zn-TCPP MOFs were further elucidated through FTIR analysis (Fig. 2B). The FTIR spectrum of the TCPP ligand displayed an absorption peak at 3310 cm^{-1} for the N—H stretching vibration and two peaks at 1604 cm^{-1} and 1100 cm^{-1} attributed to the skeletal vibrations (Zhao et al., 2018). For the bulk and exfoliated Zn-TCPP, the absence of the peak at 3310 cm^{-1}, the emergence of a new peak at 993 cm^{-1}, and the retention of two peaks at 1604 cm^{-1} and 1100 cm^{-1} from TCPP indicated the substitution of hydrogen proton with zinc ions, resulting in the formation of metalloporphyrin (Zhao et al., 2020). Comparing the FTIR spectrum of Zn-TCPP nanosheet and bulk Zn-TCPP, a stronger vibration stretching at 1255 cm^{-1} assigned to the C—O bond in the nanosheets confirmed the successful attachment of PEG onto the MOF nanosheets. The synthesized Zn-TCPP nanosheets had an approximate thickness of 0.9 nm, as shown in the AFM data (Fig. 2C), which agrees well with the theoretical thickness (0.93 nm) of a monolayer of Zn-TCPP nanosheets (Zhang et al., 2024). Furthermore, the HRTEM images (Fig. S3) displayed the ultrathin nanosheets with a crystalline structure after exfoliation.

In this synthesis process, PEG with a molecular weight of 20,000 g/mol functions as a surfactant. It selectively binds to the MOF surface after nucleation, promoting anisotropic growth (Cao et al., 2016; Zhao et al., 2015), resulting in the formation of ultrathin Zn-TCPP nanosheets (Fig. S4D). This selective binding by PEG inhibits the growth of MOFs along the stacking direction while facilitating two-dimensional expansion, ultimately leading to the formation of ultrathin MOF nanosheets. In contrast, using the traditional synthesis method without PEG results in isotropic growth, producing only bulk MOF crystals (Fig. 1A). Additionally, an added advantage of PEG-assisted exfoliation is the prevention of the aggregation of the nanosheets, as evidenced by the characteristic Tyndall effect observed in the stable colloidal suspension (Fig. S5). This suggests a feasible method for producing ultrathin monolayers of MOFs with the use of PEG, which can then be utilized to create uniform MOF interlayers for membrane fabrication.

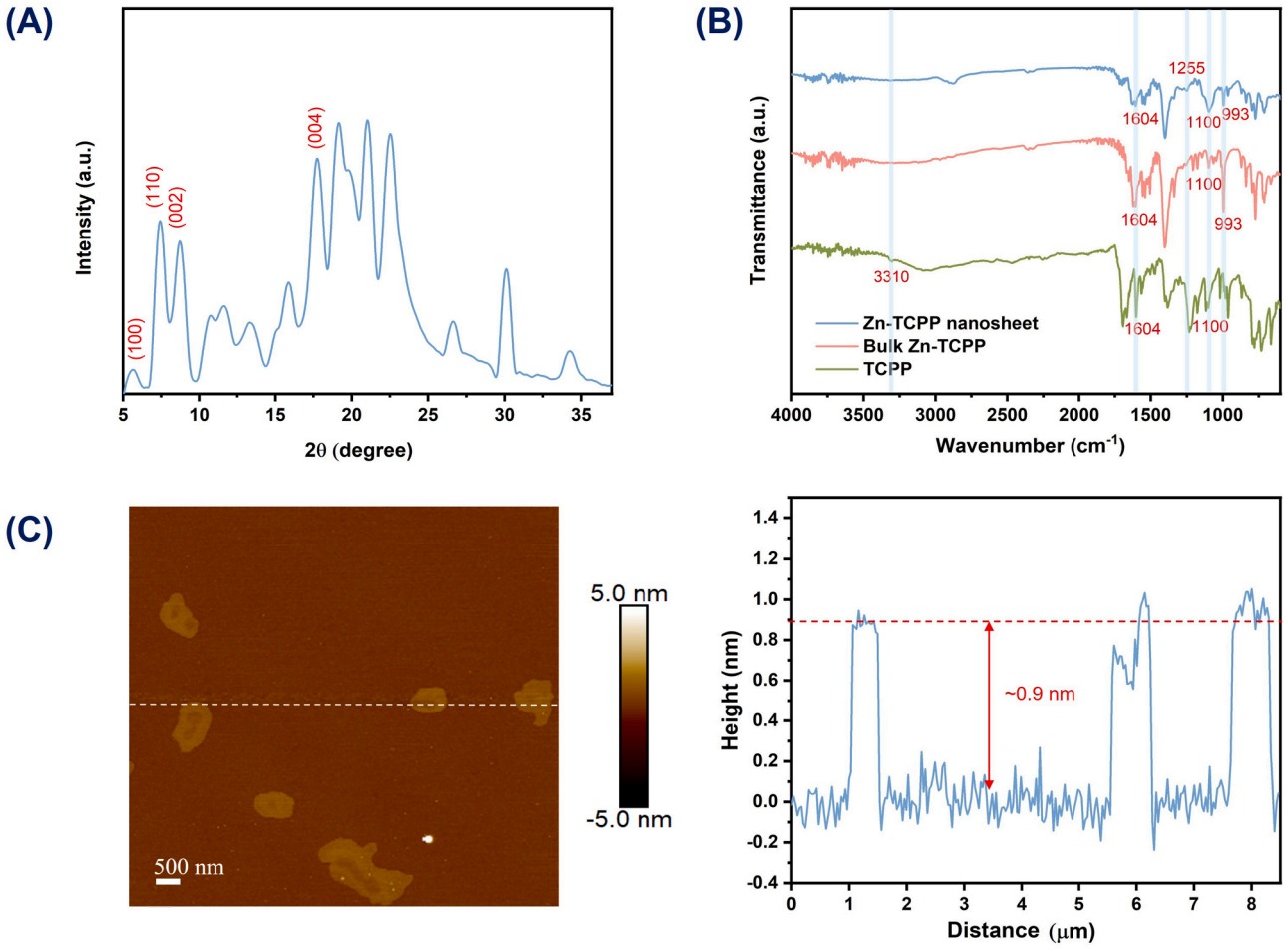

Fig. 2. (A) XRD spectra of exfoliated Zn-TCPP nanosheet. (B) FTIR spectrum of the Zn-TCPP nanosheet, bulk Zn-TCPP, and TCPP ligand. (C) AFM of the Zn-TCPP nanosheet.

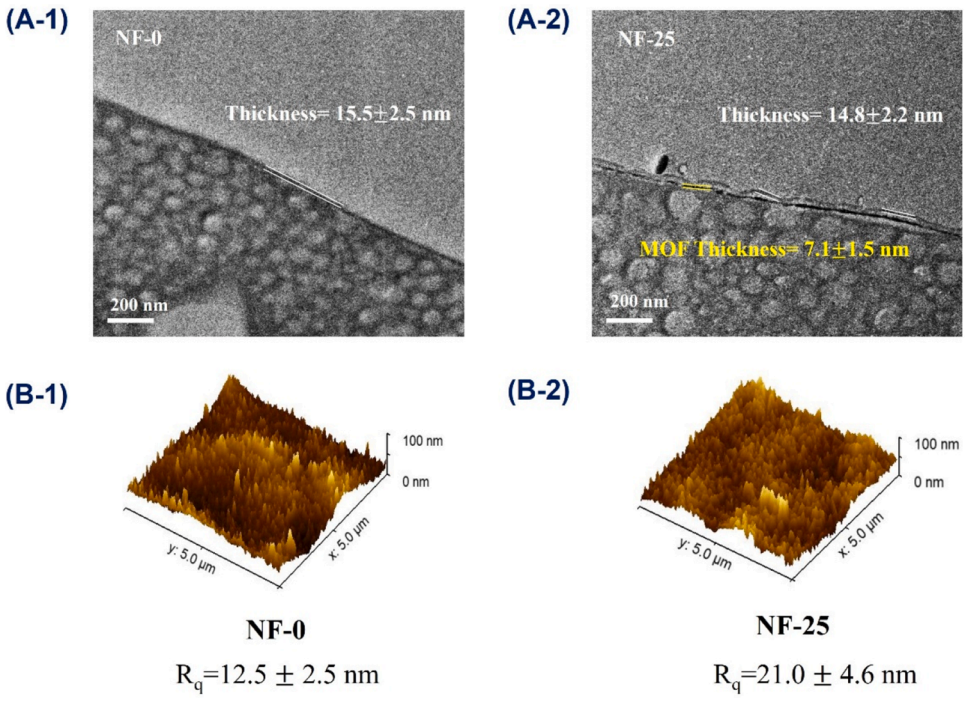

Fig. 3. TEM cross-section images of (A-1) NF-0 membrane and (A-2) NF-25 membrane. AFM micrographs of (B-1) NF-0 membrane and (B-2) NF-25 membrane.

3.2. Fabrication of MOF TFNi membranes

To confirm the successful fabrication of TFNi membranes, the cross-section of the NF-25 membrane was examined using TEM and compared to that of the control NF-0 membrane. As shown in Fig. 3A-2, a uniform and evenly distributed MOF interlayer with a thickness of 7.1 nm was noticeable between the PA layer and the PES support of NF-25, whereas only a thin layer of PA was present in NF-0. The characteristic FTIR peak at ~1620 cm^{-1} further confirmed the successful formation of the polyamide rejection layer (Fig. S6) (Tang et al., 2009). Additionally, the presence of Zn in the XPS survey spectra of NF-25 and the C=O deconvoluted peak at ~287.6 eV in its C 1 s spectra indicated the incorporation of Zn-TCPP MOF nanosheets and the formation of the polyamide layer, respectively (Fig. S7). The MOF interlayer had no obvious influence on the thickness of the PA rejection layer (Figs. 3A-1, 3A-2, S8, and S9). However, the presence of the MOF interlayers increased the membrane roughness from 12.5 ± 2.5 nm for NF-0 to 21.0 ± 4.6 nm for NF-25 (Fig. 3B-1 and 3B-2). According to the literature (Yang et al., 2020a), inclusion of an interlayer may induce a thinner PA layer as a result of reduced diffusion of PIP monomers to the reaction interface (Xu et al., 2020). On the other hand, the presence of the MOF layer may enhance the adsorption of more amine monomers; this increased monomer supply tends to promote the growth of the PA layer (Cheng et al., 2024; Zhao et al., 2022). These effects may offset each other, resulting in a nearly consistent thickness for the PA layer in the current study.

To understand the role of MOF interlayers in regulating polyamide formation and their impact on membrane properties, different amounts

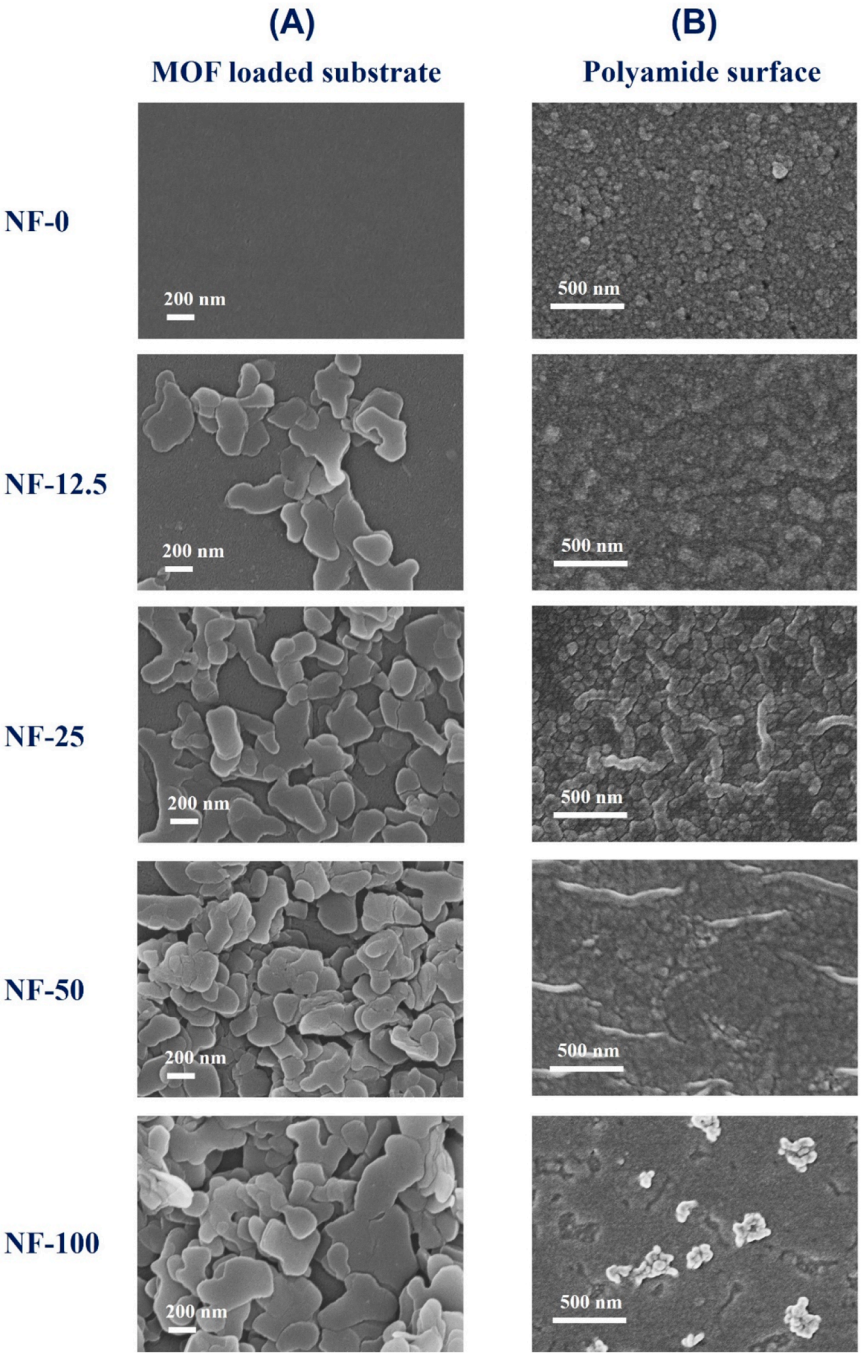

Fig. 4. SEM top view images of (A) PES substrates loaded with different amounts of MOF nanosheets; (B) Different MOF TFNi membranes.

of MOFs were tested as interlayers for constructing TFNi membranes. The surface characteristics of PES substrates coated with varying amounts of MOFs and the subsequent NF membranes were investigated, as illustrated in Fig. 4A and B. When the concentration of MOFs was low, the substrate showed incomplete coverage (e.g., PES-12.5). Optimal levels of MOF nanosheets resulted in a uniform layer across the substrate (e.g., PES-25). The incorporation of PEG as a surfactant also aided in preventing aggregation when loading MOFs. However, at higher concentrations, the nanosheets show an increased tendency to form aggregates (e.g., PES-50 and PES-100).

Regarding the fabricated NF membranes (Fig. 4B), the NF-0 control membrane without MOF interlayers exhibited a nodular-like structure typical of TFC membranes. NF-25, with the more uniformly distributed MOF interlayer, displayed a distinct stripe-like and crumpled structure, which is consistent with the increase in surface roughness observed in Fig. 3B. This morphology was possibly attributed to the enhanced confinement of degassed nanobubbles within the PA layer during the IP reaction (Gan et al., 2024; Wen et al., 2020), facilitated by the dense MOF interlayer with smaller pore sizes, leading to the formation of stripe-like features with higher roughness (Jiang et al., 2020). As for NF-50 and NF-100 with elevated MOF concentrations, the coverage of the stripes diminished gradually, likely attributed to reduced confinement effects due to nanosheet aggregation.

3.3. Membrane separation performance

As demonstrated in Fig. 5A, among all TFNi membranes, the NF-25 with the most uniform MOF coverage showed a remarkable improvement in water permeance (32.1 LMH/bar), exhibiting a threefold increase against the NF-0 control membrane (10.6 LMH/bar). This substantial improvement in water permeance could be potentially attributed to the introduction of PEG during the MOF exfoliation or the incorporation of MOF interlayers. XPS analysis (Fig. S10) revealed a higher relative content of C–O functional groups, while FTIR (Fig. S11) showed an intensified ν(C–O) vibration at 1255 cm^{-1} in Zn-TCPP nanosheets, confirming the retention of PEG on the MOF surface even after purification. To elucidate the underlying mechanisms, a control NF membrane incorporating the PEG was prepared (NF-0-PEG). As shown in Fig. S12, the NF-0-PEG membrane without the MOF interlayer exhibited only a slight increase in pure water permeance compared to NF-0, indicating that PEG had a mild effect on enhancing pure water permeance. Furthermore, a comparative study was conducted using bulk Zn-TCPP MOF as the interlayer. Despite having the same MOF concentration as NF-25, the bulk MOF-based membrane displayed significantly lower water permeance (Fig. S12). This reduction can be explained by the thicker and less uniform interlayers formed by bulk MOF, which introduce greater transport resistance compared to the well-exfoliated nanosheets in NF-25.

Hence, the observed enhancement in water permeance was mainly ascribed to the influence of interlayers on membrane formation and the facilitation of water transport (Dai et al., 2020; Yang et al., 2020b). The increased permeance could be attributed to a synergy of mechanisms: (1) the induction of a gutter effect by the interlayers, significantly diminishing the transverse resistance to water transport and overcome the unfavorable funnel effect within the polyamide layer (Long et al., 2022; Wen and Liu, 2022; Yang et al., 2020b); (2) the enhancement of the membrane's surface hydrophilicity, evidenced by a decrease in water contact angle from 33.7°±1.1° for NF-0 to 10.3°±0.4° for NF-25 (Fig. 5B), thereby fostering augmented water transport (Wei et al., 2024; Yan et al., 2016), and (3) the introduction of a more crumpled

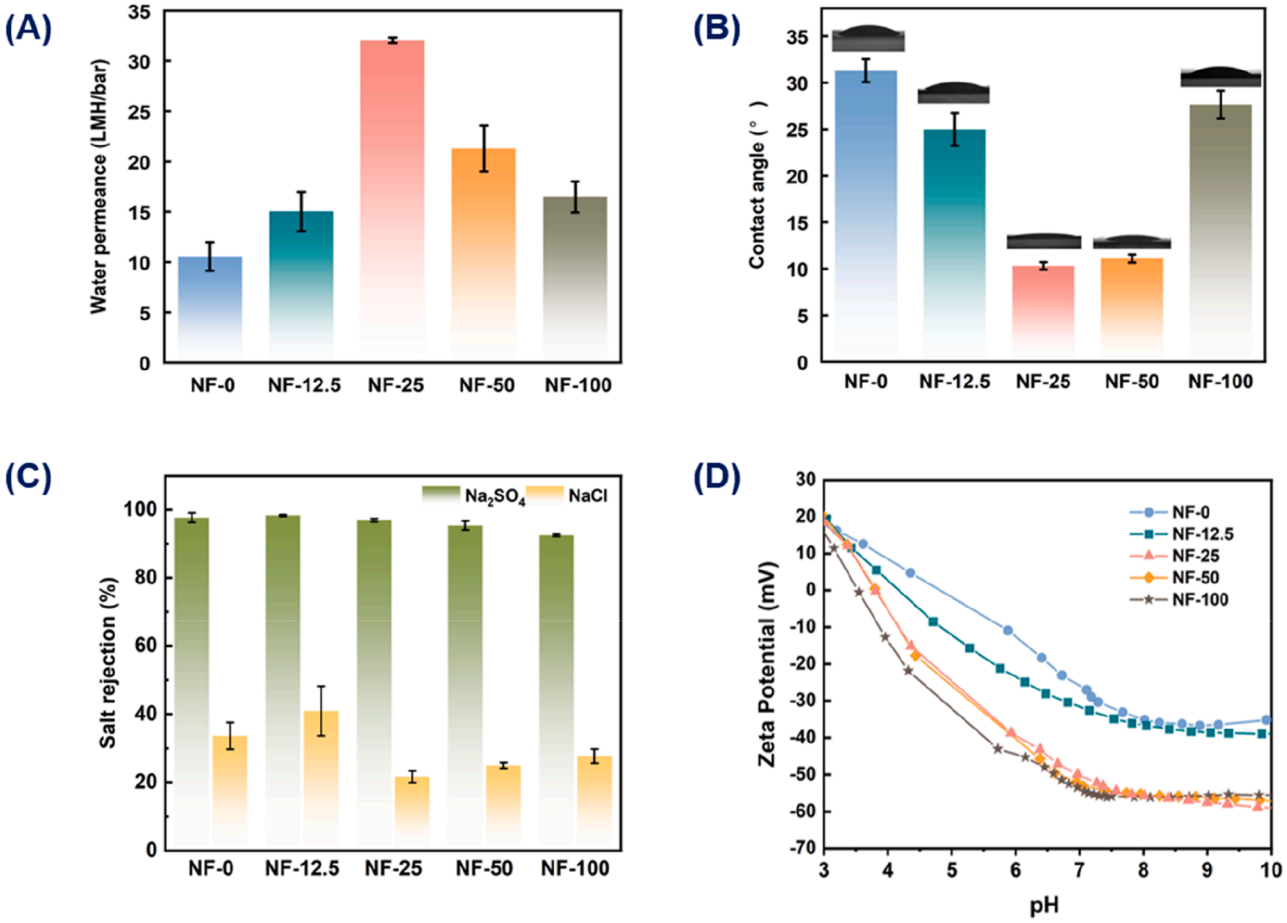

Fig. 5. (A) Pure water permeance, (B) Water contact angles, (C) Salt rejection, and (D) Zeta potential of all NF membranes.

membrane surface architecture, potentially increasing the effective filtration area accessible to water molecules (Ren et al., 2020; Shao et al., 2022). However, increasing MOF loading to form NF-50 and NF-100 resulted in decreased water permeance, possibly due to greater transport resistance caused by the thicker MOF layer.

Furthermore, the optimized NF-25 membrane demonstrated effective separation efficiency for divalent and monovalent salts, achieving a rejection of 97.0% for Na_2SO_4 and 21.7% for NaCl (Fig. 5C). This rejection difference between divalent and monovalent salts may be ascribed to the larger ionic size of sulfate ions compared to chloride ions, making them more challenging to pass through the membrane pores (Shi et al., 2021). Additionally, the stronger electrostatic repulsion between divalent ions and the negatively charged membrane surface indicated by the zeta potential results (Fig. 5D) also contributes to the higher retention of sulfate ions (Childress and Elimelech, 2000; Long et al., 2022). The NF-25 membrane also exhibited a lower rejection of NaCl than the NF-0 membrane, which can be ascribed to its slightly larger mean pore radius (0.306 nm) compared to that of the NF-0 membrane (0.293 nm) (Fig. S13). Nevertheless, the NF-25 membrane can maintain the high rejection for Na_2SO_4 attributed to its more negatively charged surface. Moreover, the NF-25 membrane maintained 97% Na_2SO_4 rejection and a relatively stable permeance over 24 h (Fig. S14), highlighting its good stability for prolonged operation.

3.4. OMPs rejection and selectivity

The rejection of OMPs including PFASs, EDCs, and PhACs, in comparison to various neutral hydrophilic surrogates, was investigated using both NF-0 and the optimized NF-25 TFNi membrane (see details in Section 2.4 and Text S1). The rejection data of these compounds were plotted against their molecular weights (Fig. 6A and B). For the neutral surrogates, their rejection is primarily determined by the size exclusion effect (Bellona et al., 2004; Mohammad et al., 2015). In the current study, the rejection of OMPs by the NF-0 membrane (Fig. 6A) was comparable to those of the neutral probes of similar molecular weights, which might suggest the important role of size exclusion (Liu et al., 2023). Some hydrophobic EDCs and PFASs were slightly below the fitted curve, which might be ascribed to the hydrophobic interactions between solutes and the membranes, thereby reducing their removal efficiency (Guo et al., 2022).

Upon comparing Fig. 6A and B, it is evident that the NF-25 membrane had a notably higher rejection of OMPs compared to the control NF-0 membrane. This heightened rejection suggests that factors beyond mere size exclusion may influence the OMP rejection process. Given that the NF-25 membrane was more negatively charged and more hydrophilic compared to the NF-0 membrane (Fig. 5B and D), it is reasonable to attribute enhanced rejection by NF-25 to stronger electrostatic repulsion and reduced hydrophobic interactions, as depicted in the schematic illustration in Fig. 6C. For instance, the negatively charged and hydrophobic PFASs exhibited a significant increase in the rejection

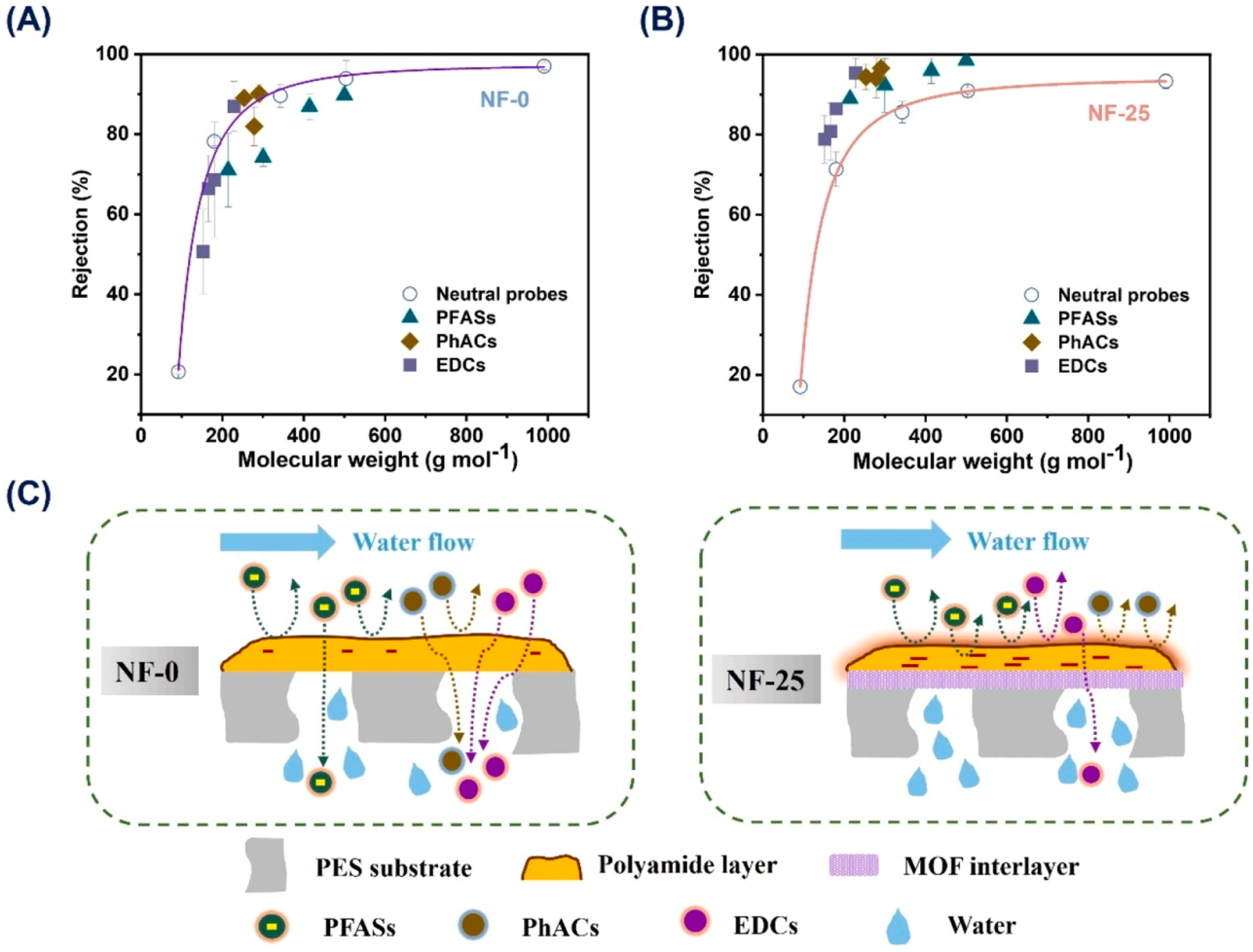

Fig. 6. Rejection of PFASs, EDCs, PhACs, and neutral probes as a function of their molecular weights of (A) NF-0 membrane and (B) NF-25 membrane. The line represents the "log-normal cdf" function fitting of the neutral probe rejection curve. (C) The modified schematic illustration of the mechanisms underlying OMP removal for the NF-0 and NF-25 membranes (Guo et al., 2022; Kim et al., 2008; Yang et al., 2020b).

compared to the neutral probes for NF-25 (Fig. 6B), further confirming the important role of the charge and hydrophilicity effects of this membrane. Additional evidence comes from the stable rejection performance during prolonged operation (Fig. S1), which demonstrates minor adsorption effects by either the membrane or nanomaterials. These results collectively demonstrate that the improved rejection performance stems primarily from the enhanced hydrophilicity and negative charge characteristics of the polyamide layer.

To evaluate the enhanced selectivity of the TFNi membrane for OMPs and to understand the underlying mechanisms, the water-solute selectivity ratio *A/B* for different OMPs was compared (Fig. 7). Notably, a prominent enhancement in selectivity was observed for hydrophobic and negatively charged PFASs as compared to PhACs and EDCs. This enhancement could be potentially attributed to the synergistic effect of increased electrostatic repulsion and hydrophobic suppression for PFASs, resulting in a more substantial reduction in *B*. Among the four PFASs studied, the reduction of *B* was particularly pronounced for PFBS and PFOS, resulting in much higher selectivity enhancements for these two compounds. The repulsion of negatively charged PFASs was significantly intensified, especially for PFBS with the lowest pKa (Table S1). Furthermore, the more hydrophilic surface impeded the attachment of hydrophobic molecules, particularly PFOS, which possesses the highest log K_{ow} (Table S1). Moreover, the NF-25 membrane exhibits excellent long-term stability over 48 h of operation (Fig. S1) and good reusability across five filtration cycles (Fig. S15).

In summary, the NF-25 TFNi membrane, which exhibited enhanced negative charge and hydrophilicity compared to the control TFC membrane, significantly improved the rejection and selectivity of all assessed OMPs. These properties would effectively reduce solute transport (lower *B* value) for charged (PFASs) or hydrophobic compounds (PFASs and EDCs). In addition, the enhanced water transport of NF-25 (greater *A* value, Fig. 5A) would also favor a higher selectivity even for neutral hydrophilic compounds (e.g., SMZ and TMP). Compared to recent studies on TFNi membranes (Table S2), the NF-25 TFNi membrane in this study demonstrates impressive performance in terms of water permeance and rejection of a substantial portion of OMPs. This highlights the promising potential of 2D MOFs as interlayers for efficient water reuse.

4. Conclusions

In this study, ultrathin Zn-TCPP MOF nanosheets with a thickness of 0.9 nm were successfully exfoliated using a PEG-assisted synthesis approach, and the resulting MOF nanosheets were employed as interlayers for constructing TFNi membranes. The NF-25 TFNi membrane, with the most uniformly distributed MOF interlayers, exhibited a strip-like and crumpled surface morphology compared to the pristine TFC membrane. It demonstrated a significant enhancement in water permeance and OMP selectivity (particularly for PFASs) compared to conventional TFC membranes. The observed increase in water permeance can be attributed to the gutter effect, alongside a more hydrophilic and crumpled surface morphology. Additionally, the improved OMP selectivity may be linked to a more hydrophilic and negatively charged surface that suppresses solute permeance. This work provides new insight into the fabrication of high-performance MOF TFNi membranes using a novel PEG-assisted exfoliation method to mitigate MOF restacking and aggregation issues. The findings from this study also deepen our understanding of OMP removal mechanisms regarding MOF TFNi membranes and pave the way for the broader application of these membranes in OMP removal and water reuse.

CRediT authorship contribution statement

Ruiying Li: Writing – original draft, Methodology, Investigation, Formal analysis, Data curation, Conceptualization. **Lingyue Zhang:** Writing – review & editing, Validation, Supervision, Methodology, Conceptualization. **Shuang Zheng:** Formal analysis. **Wenyu Liu:** Investigation, Formal analysis. **Li Long:** Investigation, Formal analysis. **Chuyang Tang:** Writing – review & editing, Supervision, Funding acquisition.

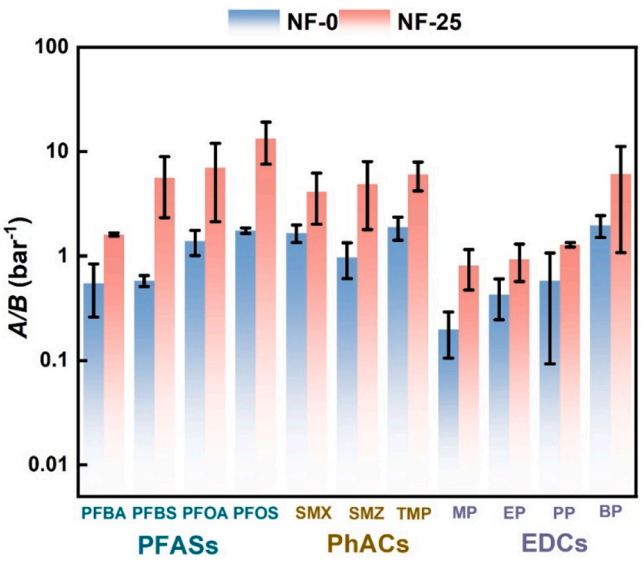

Fig. 7. Selectivity *A/B* of OMPs for NF-0 and NF-25.

Declaration of competing interest

The authors declare that they have no known competing financial interests or personal relationships that could have appeared to influence the work reported in this paper.

Acknowledgments

The work was substantially supported by grants from the Research Grants Council of the Hong Kong Special Administration Region, China (GRF 17201921, CRF C1003-23Y, and SRFS2021-7S04). The authors also acknowledge the partial support from the Seed Funding for Strategic Interdisciplinary Research Scheme (102010174) of the University of Hong Kong.

Supplementary materials

Supplementary material associated with this article can be found, in the online version, at doi:10.1016/j.watres.2025.123852.

Data availability

Data will be made available on request.

References

Ahmad, N.N.R., Ang, W.L., Teow, Y.H., Mohammad, A.W., Hilal, N., 2022. Nanofiltration membrane processes for water recycling, reuse and product recovery within various industries: a review. J. Water Process Eng. 45, 102478.

Alemayehu, H.G., Liu, C., Hou, J., Yang, J., Fang, M., Tang, Z., Li, L., 2022. Highly stable membrane comprising MOF nanosheets and graphene oxide for ultra-permeable nanofiltration. J. Membr. Sci. 652, 120479.

Barbosa, M.O., Moreira, N.F., Ribeiro, A.R., Pereira, M.F., Silva, A.M., 2016. Occurrence and removal of organic micropollutants: an overview of the watch list of EU Decision 2015/495. Water Res. 94, 257–279.

Bellona, C., Drewes, J.E., Xu, P., Amy, G., 2004. Factors affecting the rejection of organic solutes during NF/RO treatment–a literature review. Water Res. 38 (12), 2795–2809.

Bhatt, P., Bhandari, G., Bilal, M., 2022. Occurrence, toxicity impacts and mitigation of emerging micropollutants in the aquatic environments: recent tendencies and perspectives. J. Environ. Chem. Eng. 10 (3), 107598.

Braeken, L., Ramaekers, R., Zhang, Y., Maes, G., Van der Bruggen, B., Vandecasteele, C., 2005. Influence of hydrophobicity on retention in nanofiltration of aqueous solutions containing organic compounds. J. Membr. Sci. 252 (1–2), 195–203.
Cao, F., Zhao, M., Yu, Y., Chen, B., Huang, Y., Yang, J., Cao, X., Lu, Q., Zhang, X., Zhang, Z., 2016. Synthesis of two-dimensional $CoS_{1.097}$/Nitrogen-doped carbon nanocomposites using metal–organic framework nanosheets as precursors for supercapacitor application. J. Am. Chem. Soc. 138 (22), 6924–6927.
Cheng, P., Liu, Y., Wang, X., Fan, K., Li, P., Xia, S., 2022. Regulating interfacial polymerization via constructed 2D metal-organic framework interlayers for fabricating nanofiltration membranes with enhanced performance. Desalination 544, 116134.
Cheng, P., Liu, Y., Wei, X., Fan, K., Xia, S., 2024. Distinct efficacies of interlayers in tailoring polyamide nanofiltration membrane performance for organic micropollutant removal: dependent on substrate characteristics. Environ. Sci. Technol. 58 (31), 14022–14033.
Childress, A.E., Elimelech, M., 2000. Relating nanofiltration membrane performance to membrane charge (electrokinetic) characteristics. Environ. Sci. Technol. 34 (17), 3710–3716.
Dai, R., Li, J., Wang, Z., 2020. Constructing interlayer to tailor structure and performance of thin-film composite polyamide membranes: a review. Adv. Colloid Interface Sci. 282, 102204.
Eggen, R.I., Hollender, J., Joss, A., Schärer, M., Stamm, C., 2014. Reducing the discharge of micropollutants in the aquatic environment: the benefits of upgrading wastewater treatment plants. Environ. Sci. Technol. 48 (14), 7683–7689.
Fang, Y., Zhu, C.Y., Yang, H.C., Zhang, C., Xu, Z.K., 2024. Polyamide nanofiltration membranes by vacuum-assisted interfacial polymerization: broad universality of substrate, wide window of monomer concentration and high reproducibility of performance. J. Colloid Interface Sci. 655, 327–334.
Gan, Q., Hu, Y., Wu, C., Yang, Z., Peng, L.E., Tang, C.Y., 2024. Nanofoamed polyamide membranes: mechanisms, developments, and environmental implications. Environ. Sci. Technol. 58 (47), 20812–20829.
Garg, S., Kumar, P., Mishra, V., Guijt, R., Singh, P., Dumée, L.F., Sharma, R.S., 2020. A review on the sources, occurrence and health risks of per-/poly-fluoroalkyl substances (PFAS) arising from the manufacture and disposal of electric and electronic products. J. Water Process Eng. 38, 101683.
Guo, H., Dai, R., Xie, M., Peng, L.E., Yao, Z., Yang, Z., Nghiem, L.D., Snyder, S.A., Wang, Z., Tang, C.Y., 2022. Tweak in puzzle: tailoring membrane chemistry and structure toward targeted removal of organic micropollutants for water reuse. Environ. Sci. Technol. Lett. 9 (4), 247–257.
Guo, H., Deng, Y., Tao, Z., Yao, Z., Wang, J., Lin, C., Zhang, T., Zhu, B., Tang, C.Y., 2016. Does hydrophilic polydopamine coating enhance membrane rejection of hydrophobic endocrine-disrupting compounds? Environ. Sci. Technol. Lett. 3 (9), 332–338.
Guo, H., Yao, Z., Yang, Z., Ma, X., Wang, J., Tang, C.Y., 2017. A one-step rapid assembly of thin film coating using green coordination complexes for enhanced removal of trace organic contaminants by membranes. Environ. Sci. Technol. 51 (21), 12638–12643.
Ji, C., Zhai, Z., Jiang, C., Hu, P., Zhao, S., Xue, S., Yang, Z., He, T., Niu, Q.J., 2021. Recent advances in high-performance TFC membranes: a review of the functional interlayers. Desalination 500, 114869.
Jiang, C., Zhang, L., Li, P., Sun, H., Hou, Y., Niu, Q.J., 2020. Ultrathin film composite membranes fabricated by novel *in situ* free interfacial polymerization for desalination. ACS Appl. Mater. Interfaces 12 (22), 25304–25315.
Jin, X.G., Liang, X.K., Liu, J.H., Mo, J.W., Ren, T.X., Ma, X.H., Xu, Z.L., 2023. Development of high permeability nanofiltration membranes through porous 2D MOF nanosheets. Chem. Eng. J. 471, 144566.
Khanzada, N.K., Farid, M.U., Kharraz, J.A., Choi, J., Tang, C.Y., Nghiem, L.D., Jang, A., An, A.K., 2020. Removal of organic micropollutants using advanced membrane-based water and wastewater treatment: a review. J. Membr. Sci. 598, 117672.
Kim, J.H., Park, P.K., Lee, C.H., Kwon, H.H., 2008. Surface modification of nanofiltration membranes to improve the removal of organic micro-pollutants (EDCs and PhACs) in drinking water treatment: graft polymerization and cross-linking followed by functional group substitution. J. Membr. Sci. 321 (2), 190–198.
Kimura, K., Amy, G., Drewes, J., Watanabe, Y., 2003. Adsorption of hydrophobic compounds onto NF/RO membranes: an artifact leading to overestimation of rejection. J. Membr. Sci 221 (1–2), 89–101.
Lapworth, D., Baran, N., Stuart, M., Ward, R., 2012. Emerging organic contaminants in groundwater: a review of sources, fate and occurrence. Environ. Pollut. 163, 287–303.
Lau, W., Gray, S., Matsuura, T., Emadzadeh, D., Chen, J.P., Ismail, A., 2015. A review on polyamide thin film nanocomposite (TFN) membranes: history, applications, challenges and approaches. Water Res. 80, 306–324.
Li, P.Z., Maeda, Y., Xu, Q., 2011. Top-down fabrication of crystalline metal-organic framework nanosheets. Chem. Commun. (Camb.) 47 (29), 8436–8438.
Li, X., Liu, Y., Wang, J., Gascon, J., Li, J., Van der Bruggen, B., 2017. Metal–organic frameworks based membranes for liquid separation. Chem. Soc. Rev. 46 (23), 7124–7144.
Liu, W., Long, L., Yang, Z., Wang, L., Gan, Q., Zhou, S., Sarkar, P., Guo, H., Tang, C.Y., 2023. Enhancing the removal of organic micropollutants by nanofiltration membrane with Fe (III)-tannic acid interlayer: mechanisms and environmental implications. Water Res. 245, 120623.
Liu, Y., Wang, K., Zhou, Z., Wei, X., Xia, S., Wang, X.M., Xie, Y.F., Huang, X., 2022. Boosting the performance of nanofiltration membranes in removing organic micropollutants: trade-off effect, strategy evaluation, and prospective development. Environ. Sci. Technol. 56 (22), 15220–15237.
Long, L., Wu, C., Yang, Z., Tang, C.Y., 2022. Carbon nanotube interlayer enhances water permeance and antifouling performance of nanofiltration membranes: mechanisms and experimental evidence. Environ. Sci. Technol. 56 (4), 2656–2664.
Luo, Y., Guo, W., Ngo, H.H., Nghiem, L.D., Hai, F.I., Zhang, J., Liang, S., Wang, X.C., 2014. A review on the occurrence of micropollutants in the aquatic environment and their fate and removal during wastewater treatment. Sci. Total Environ. 473, 619–641.
Mohammad, A.W., Teow, Y., Ang, W., Chung, Y., Oatley-Radcliffe, D., Hilal, N., 2015. Nanofiltration membranes review: recent advances and future prospects. Desalination 356, 226–254.
Price, O.R., Hughes, G.O., Roche, N.L., Mason, P.J., 2010. Improving emissions estimates of home and personal care products ingredients for use in EU risk assessments. Integr. Environ. Assess. Manag. 6 (4), 677–684.
Ren, L., Chen, J., Lu, Q., Wang, C., Han, J., Huang, K., Pan, X., Wu, H., 2020. Construction of high selectivity and antifouling nanofiltration membrane via incorporating macrocyclic molecules into active layer. J. Membr. Sci. 597, 117641.
Rodenas, T., Luz, I., Prieto, G., Seoane, B., Miro, H., Corma, A., Kapteijn, F., Llabres, I.X. F.X., Gascon, J., 2015. Metal-organic framework nanosheets in polymer composite materials for gas separation. Nat. Mater. 14 (1), 48–55.
Schafer, A.I., Akanyeti, I., Semiao, A.J., 2011. Micropollutant sorption to membrane polymers: a review of mechanisms for estrogens. Adv. Colloid Interface Sci. 164 (1–2), 100–117.
Shao, S., Zeng, F., Long, L., Zhu, X., Peng, L.E., Wang, F., Yang, Z., Tang, C.Y., 2022. Nanofiltration membranes with crumpled polyamide films: a critical review on mechanisms, performances, and environmental applications. Environ. Sci. Technol. 56 (18), 12811–12827.
Shi, Y.T., Meng, X., Yao, L., Tian, M., 2021. A full-scale study of nanofiltration: separation and recovery of NaCl and Na2SO4 from coal chemical industry wastewater. Desalination 517, 115239.
Tang, C.Y., Kwon, Y.N., Leckie, J.O., 2009. Effect of membrane chemistry and coating layer on physiochemical properties of thin film composite polyamide RO and NF membranes: I. FTIR and XPS characterization of polyamide and coating layer chemistry. Desalination 242 (1–3), 149–167.
Tang, C.Y., Yang, Z., Guo, H., Wen, J.J., Nghiem, L.D., Cornelissen, E., 2018. Potable water reuse through advanced membrane technology. Environ. Sci. Technol. 52, 10215–10223.
Tran, N.H., Reinhard, M., Gin, K.Y., 2018. Occurrence and fate of emerging contaminants in municipal wastewater treatment plants from different geographical regions-a review. Water Res. 133, 182–207.
Wang, A., Xu, H., Fu, J., Lin, T., Ma, J., Ding, M., Gao, L., 2023. Enhanced high-salinity brines treatment using polyamide nanofiltration membrane with tunable interlayered MXene channel. Sci. Total Environ. 856, 158434.
Wang, T., Wang, J., Zhao, Z., Zheng, X., Li, J., Liu, H., Zhao, Z., 2021. Bio-inspired fabrication of anti-fouling and stability of nanofiltration membranes with a poly (dopamine)/graphene oxide interlayer. Ind. Eng. Chem. Res. 60 (41), 14868–14883.
Wang, X., Lyu, Q., Tong, T., Sun, K., Lin, L.C., Tang, C.Y., Yang, F., Guiver, M.D., Quan, X., Dong, Y., 2022. Robust ultrathin nanoporous MOF membrane with intra-crystalline defects for fast water transport. Nat. Commun. 13 (1), 266.
Wei, X., Fan, K., Cheng, P., Liu, Y., Xia, S., 2024. Modification of nanofiltration membranes using beta-cyclodextrin derivatives with different functional groups for enhanced removal of organic micropollutants. Desalination 573, 117219.
Wen, H., Liu, C., 2022. Effect of the interlayer construction on the performances of the TFC-FO membranes: a review from materials perspective. Desalination 541, 116033.
Wen, Y., Zhang, X., Li, X., Wang, Z., Tang, C.Y., 2020. Metal–organic framework nanosheets for thin-film composite membranes with enhanced permeability and selectivity. ACS Appl. Nano Mater. 3 (9), 9238–9248.
Xu, D., Zhu, X., Luo, X., Guo, Y., Liu, Y., Yang, L., Tang, X., Li, G., Liang, H., 2020. MXene nanosheet templated nanofiltration membranes toward ultrahigh water transport. Environ. Sci. Technol. 55 (2), 1270–1278.
Yan, F., Chen, H., Lü, Y., Lü, Z., Yu, S., Liu, M., Gao, C., 2016. Improving the water permeability and antifouling property of thin-film composite polyamide nanofiltration membrane by modifying the active layer with triethanolamine. J. Membr. Sci. 513, 108–116.
Yang, Z., Sun, P.F., Li, X., Gan, B., Wang, L., Song, X., Park, H.D., Tang, C.Y., 2020a. A critical review on thin-film nanocomposite membranes with interlayered structure: mechanisms, recent developments, and environmental applications. Environ. Sci. Technol. 54 (24), 15563–15583.
Yang, Z., Wang, F., Guo, H., Peng, L.E., Ma, X.H., Song, X.X., Wang, Z., Tang, C.Y., 2020b. Mechanistic insights into the role of polydopamine interlayer toward improved separation performance of polyamide nanofiltration membranes. Environ. Sci. Technol. 54 (18), 11611–11621.
Zhang, L., Li, R., Zheng, S., Zhu, H., Cao, M., Li, M., Hu, Y., Long, L., Feng, H., Tang, C.Y., 2024. Hydrogel-embedded vertically aligned metal-organic framework nanosheet membrane for efficient water harvesting. Nat. Commun. 15 (1), 9738.
Zhao, B., Guo, Z., Wang, H., Wang, L., Qian, Y., Long, X., Ma, C., Zhang, Z., Li, J., Zhang, H., 2021. Enhanced water permeance of a polyamide thin-film composite nanofiltration membrane with a metal-organic framework interlayer. J. Membr. Sci. 625, 119154.
Zhao, F., Hao, Y., Xu, Q., Hao, Z., Li, X., Cheng, L., Chen, D., Shi, X., Xiao, Y., Wei, P., 2023. Safety assessment of organic micropollutants in reclaimed water: chemical analyses, ecological risk assessments, and *in vivo* endocrine-disrupting studies. Sci. Total Environ. 884, 163865.
Zhao, M., Wang, Y., Ma, Q., Huang, Y., Zhang, X., Ping, J., Zhang, Z., Lu, Q., Yu, Y., Xu, H., Zhao, Y., Zhang, H., 2015. Ultrathin 2D metal-organic framework nanosheets. Adv. Mater. 27 (45), 7372–7378.

Zhao, Y., Jiang, L., Shangguan, L., Mi, L., Liu, A., Liu, S., 2018. Synthesis of porphyrin-based two-dimensional metal–organic framework nanodisk with small size and few layers. J. Mater. Chem. A 6 (6), 2828–2833.
Zhao, Y., Tong, X., Kim, J., Tong, T., Huang, C.H., Chen, Y., 2022. Capillary-assisted fabrication of thin-film nanocomposite membranes for improved solute–solute separation. Environ. Sci. Technol. 56 (9), 5849–5859.
Zhao, Y., Wang, J., Pei, R., 2020. Micron-sized ultrathin metal-organic framework sheet. J. Am. Chem. Soc. 142 (23), 10331–10336.
Zhou, H., Qiu, Z., Zeng, J., Dai, R., Wang, Z., 2023. Ultra-permeable polyamide nanofiltration membrane modified by hydrophilic-hydrophobic alternated lignocellulosic nanofibrils for efficient water reuse. J. Membr. Sci. 688, 122125.
Zhu, C.Y., Li, H.N., Yang, J., Li, J.J., Ye, J.R., Xu, Z.K., 2020. Vacuum-assisted diamine monomer distribution for synthesizing polyamide composite membranes by interfacial polymerization. J. Membr. Sci. 616, 118557.